ACS NANO
Cite This: ACS Nano 2017, 11, 10366-10372
www.acsnano.org

ARTICLE

Anomalous Polarized Raman Scattering and Large Circular Intensity Differential in Layered Triclinic ReS_2

Shishu Zhang, Nannan Mao, Na Zhang, Juanxia Wu, Lianming Tong,* and Jin Zhang*

Center for Nanochemistry, Beijing Science and Engineering Center for Nanocarbons, Beijing National Laboratory for Molecular Sciences, College of Chemistry and Molecular Engineering, Peking University, Beijing 100871, China

Supporting Information

ABSTRACT: The Raman tensor of a crystal is the derivative of its polarizability tensor and is dependent on the symmetries of the crystal and the Raman-active vibrational mode. The intensity of a particular mode is determined by the Raman selection rule, which involves the Raman tensor and the polarization configurations. For anisotropic two-dimensional (2D) layered crystals, polarized Raman scattering has been used to reveal the crystalline orientations. However, due to its complicated Raman tensors and optical birefringence, the polarized Raman scattering of triclinic 2D crystals has not been well studied yet. Herein, we report the anomalous polarized Raman scattering of 2D layered triclinic rhenium disulfide (ReS_2) and show a large circular intensity differential (CID) of Raman scattering in ReS_2 of different thicknesses. The origin of CID and the anomalous behavior in polarized Raman scattering were attributed to the appearance of nonzero off-diagonal Raman tensor elements and the phase factor owing to optical birefringence. This can provide a method to identify the vertical orientation of triclinic layered materials. These findings may help to further understand the Raman scattering process in 2D materials of low symmetry and may indicate important applications in chiral recognition by using 2D materials.

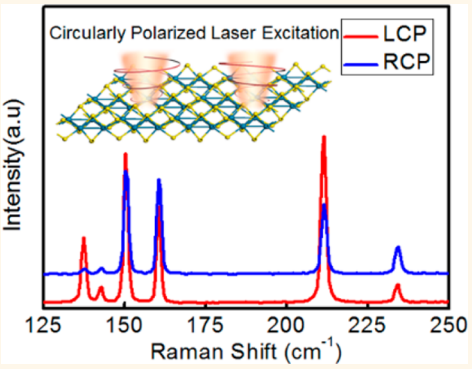

KEYWORDS: *polarized Raman scattering, circular intensity differential, triclinic, rhenium disulfide, birefringence*

Raman spectroscopy is a rapid and nondestructive method to characterize two-dimensional (2D) layered materials.[1−4] According to the Raman selection rule $I \propto |e_s \cdot R \cdot e_i|^2$, the intensity of a Raman-active phonon mode is determined by the Raman tensor (R) and the polarization configurations (e_i, e_s). For anisotropic 2D layered materials, due to the reduced in-plane symmetry, the intensities of the Raman-active modes are polarization-dependent and change periodically with polarization angle.[5−9] As a result, angle-resolved polarized Raman scattering has been developed for the identification of the crystal orientation of anisotropic few-layered 2D materials.[6,7] Further studies also suggested that the photon−electron and electron−phonon interactions have to be taken into account for reliable identification.[5,10]

The polarizability tensor of anisotropic crystals has off-diagonal elements, and the form of the Raman tensor of a Raman-active phonon mode depends on the lattice vibrational symmetry and the symmetry of the crystal.[1] For example, for hexagonal crystals such as MoS_2 (D_{6h}, $P6_3/mmc$),[11,12] the A_{1g} mode has the Raman tensor of $\begin{bmatrix} u & 0 \\ 0 & u \end{bmatrix}$ in two dimensions and showed no polarization-dependence under both parallel and perpendicular configurations. However, for crystals with reduced symmetry, such as orthorhombic black phosphorus (D_{2h}, $Cmca$)[6,12,13] or monoclinic molybdenum ditelluride,[14] the Raman tensor of the A_g mode is $\begin{bmatrix} u & 0 \\ 0 & w \end{bmatrix}$ and the angle-dependent Raman scattering efficiency is given by $I_{\parallel} \propto (u \cos^2 \theta + w \sin^2 \theta)^2$ under parallel polarization configuration according to the Raman selection rule. Further reducing the crystal symmetry, one can find the Raman tensor of the A_g mode in triclinic crystals such as ReS_2 (C_i, $P\bar{1}$), $R = \begin{bmatrix} u & v \\ v & w \end{bmatrix}$, where the off-diagonal elements appear and the Raman tensor is now defined by three parameters (u, v, w),[15] rather than the single parameter (u) in hexagonal MoS_2. As a result, the angle-resolved polarized Raman scattering of triclinic 2D materials is more difficult to predict. Furthermore, due to the anisotropic optical properties in 2D materials of low symmetry, including the optical absorption and birefringence, the polarization states of the incident and scattered light can be altered after passing through the samples, particularly if the sample is relatively thick.

Received: July 27, 2017
Accepted: October 9, 2017
Published: October 9, 2017

DOI: 10.1021/acsnano.7b05321
ACS Nano 2017, 11, 10366−10372

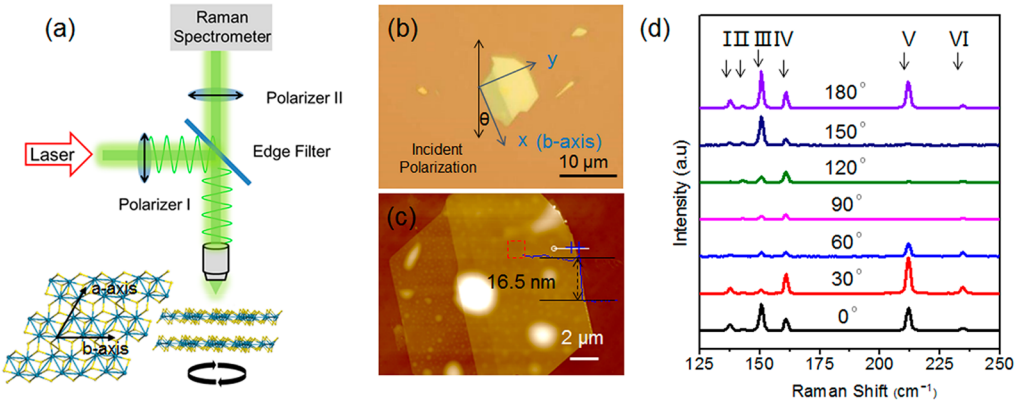

Figure 1. (a) Schematic of the angle-resolved polarized Raman spectroscopy. The inset is the top view of the ReS_2 crystal structure. (b) Optical image of the ReS_2 sample. θ is defined as the angle between the *b*-axis of ReS_2 and the incident polarization. (c) Corresponding atomic force micrograph (AFM) of the ReS_2 sample. (d) Raman spectra of the ReS_2 sample with different rotation angles under 514.5 nm laser excitation.

Although the optical effects have been studied in orthorhombic BP,[16] it is more complex for biaxial triclinic crystals and may lead to exceptional behavior in Raman scattering.

Since its discovery as a 2D layered transition metal dichalcogenide, ReS_2 has attracted much attention in recent years owing to its crystal structure and strong in-plane anisotropy in electrical and optical properties, such as electrical transport,[17,18] optoelectronic response,[19] photoluminescence,[20] optical absorption,[19] and Raman scattering.[13,15,21−23] ReS_2 has a distorted 1T′ phase with triclinic symmetry.[24,25] The polarized Raman spectra of ReS_2 have been measured and used to identify the direction of Re−Re chains;[21] however, the systematical study of polarized Raman scattering in ReS_2 has not been performed yet.

Herein, we report the anomalous polarized Raman scattering of layered triclinic ReS_2. Due to the appearance of nonzero off-diagonal elements of the Raman tensor and optical birefringence effect, the polar plots of angle-resolved polarized Raman spectra showed twisted butterfly-like patterns, and the direction of the maxima of mode V (212 cm^{-1}) showed significant deviation from the *b*-axis of ReS_2. This phenomenon was explained by using the model of Raman scattering efficiency taking into account the nonzero Raman tensor elements and the modulation of the polarization states of incident and scattered light by the Jones matrix. More importantly, upon excitation by a circularly polarized laser, the ReS_2 flakes showed significantly different response to different circularly polarized laser excitation. The circular intensity differential (CID) in ReS_2 was on the order of 10^{-1}. The large CID can provide a method to identify the vertical orientation of triclinic layered materials. These findings not only suggested a general physical model to describe the polarized Raman scattering of anisotropic 2D layered materials but also indicated the possibility of chiral recognition using 2D layered materials.

RESULTS AND DISCUSSION

Figure 1a illustrates the optical layout of the angle-resolved polarized Raman scattering measurements. As shown in the scheme, the polarization of the incident laser was selected by the polarizer, and an analyzer was placed in front of the detector. The polarization configuration can be set as either parallel or cross by rotating the analyzer. The polarized Raman spectra were recorded in a backscattering geometry at different rotation angles of the sample. The crystal structure of ReS_2 is shown in the inset of Figure 1a. The zigzag chain of Re−Re bonds is defined as the *b*-axis of the crystal.[18,24,26] Figure 1b shows the optical image of a few-layered ReS_2 sample mechanically exfoliated on a 300 nm SiO_2/Si substrate. The clear and sharp edges of exfoliated ReS_2 have been proven to be along the *b*-axis.[15,21] In Figure 1b, the *b*-axis is defined as the *x* direction in the experimental coordinate, the *y* direction is perpendicular to the *b*-axis, and θ is the angle between the directions of the *b*-axis and the incident polarization.

According to the group theory, bulk ReS_2 belongs to the C_i point group and $P\bar{1}$ space group (Figure S1). Because of the Re_4 parallelogram, there are 12 atoms in a ReS_2 unit cell, so it has 36 phonon modes including 18 A_g modes and 18 A_u modes. All the A_g modes are Raman-active, and the 18 A_u modes include 15 infrared-active modes and three acoustic A_u modes.[25] All the A_g modes are detectable, and the Raman peaks appear in the range of 100−450 cm^{-1} (Figure S2). The six peaks below 250 cm^{-1}, including 137.9 cm^{-1} (defined as mode I), 143.3 cm^{-1} (mode II), 150.7 cm^{-1} (mode III), 161.0 cm^{-1} (mode IV), 212.8 cm^{-1} (mode V), and 234.7 cm^{-1} (mode VI), are assigned to the lattice vibrations related to the motion of Re atoms. In this work, we focus on the typical Raman peaks below 250 cm^{-1} because of their high intensities, which were usually used to characterize 2D ReS_2 samples *via* CVD growth.[27−29]

Figure 1c shows the AFM image of the sample with 7 and 16.5 nm thickness at different areas. The polarized Raman spectra were measured in the area highlighted by the red square. Figure 1d shows the Raman spectra of ReS_2 at different rotation angles under parallel polarization configuration. 0° is an arbitrary angle corresponding to the sample position shown in Figure 1b. It is seen that the intensities of all the Raman-active modes changed periodically with the rotation angle, showing a period of 180°, but their maxima corresponding to different rotation angles. According to the classical Raman selection rules,[2,11,12] the Raman intensity is proportional to $|e_s \cdot R \cdot e_i|^2$, where e_i and e_s represent the unit vectors of the incident and scattered electric fields, respectively, and can be expressed by Jones vectors.[30] Under parallel configuration, $e_i = e_s = [\cos\theta \ \sin\theta]$. *R* is the second-rank polarizability tensor of the Raman-active mode, the so-called Raman tensor.[12] ReS_2 belongs to the triclinic crystal system, and the Raman tensor of the A_g mode is described as

DOI: 10.1021/acsnano.7b05321
ACS Nano 2017, 11, 10366−10372

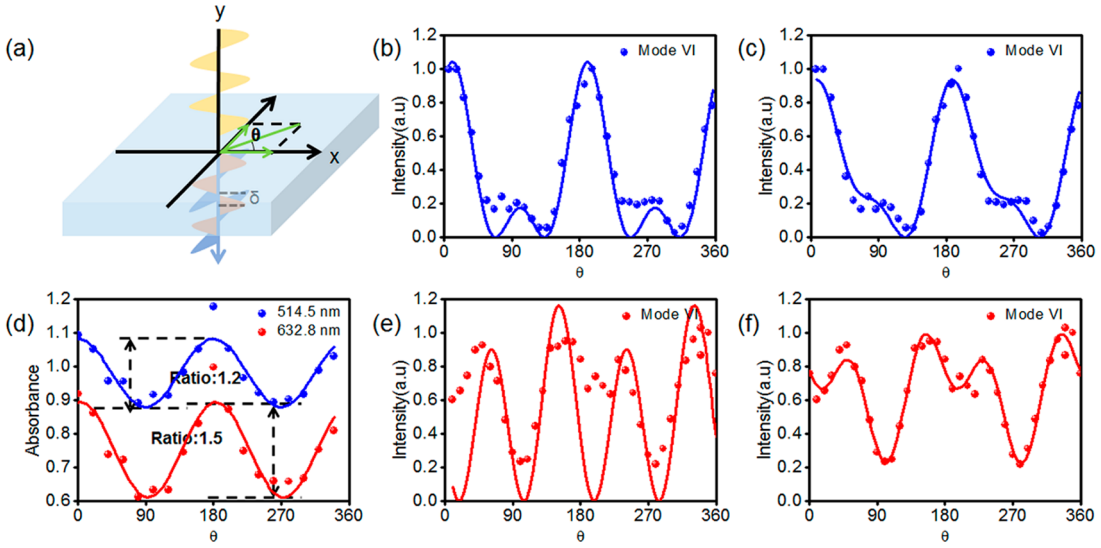

Figure 2. (a) Schematic of the optical birefringence effect, where θ is the sample rotation angle and δ is the phase delay due to the birefringence. (b, c) Angle-resolved polarized Raman spectra of mode VI under 514.5 nm laser and parallel configuration. The dots are experimental data. The solid line is the best fit to the data using eq 1 (b) and eq 3 (c). (d) Angle-resolved polarized absorption spectra of a ReS_2 flake on fused silica substrate under 514.5 and 632.8 nm laser excitation. (e, f) Angle-resolved polarized Raman spectra of mode VI under 632.8 nm laser excitation and parallel configuration. The dots are experimental data. The solid line is the best fit to the data using eq 1 (e) and eq 3 (f).

$$R = \begin{bmatrix} u & v \\ v & w \end{bmatrix}$$

in two dimensions.[15] The angular dependence of the Raman intensity of ReS_2 under parallel polarization configuration can then be written as

$$I_{\parallel} \propto (u \cos^2\theta + 2v \cos\theta \sin\theta + w \sin^2\theta)^2 \quad (1)$$

where the periodicity can be found from the maxima and minima at angles defined by the absolute values of the tensor elements (u, v, w).

The anomalous polarized Raman spectra have been observed in black phosphorus and have been interpreted by the modulation of either the Raman tensor or the electric fields.[5,6,16] Considering the absorptive nature of the material, complex Raman tensor elements with imaginary parts, which account for the optical absorption, were introduced to explain the anomalous polarized Raman scattering.[5,6] Considering the optical birefringence effect of the anisotropic crystal, the electrical fields of the incident and scattered light are expected to be altered, and the anomalous behavior can be explained by the modulation of the electric fields.[16] In this work, we considered the impacts of both optical absorption and birefringence effects in our model. We compared the angle-resolved polarized Raman spectra of ReS_2 with the same sample thickness on a 300 nm SiO_2/Si substrate and 1 mm fused silica substrate, as shown in S4 to prove that the anisotropic interference enhancement is not the key factor of anomalous polarization dependence. A detailed discussion of these two effects under both parallel and cross-polarization configurations is given in S5 and S6 in the Supporting Information.

Considering the change of the polarization states by the anisotropic materials (Figure 2a), the Jones matrix was introduced to modify the electric fields:

$$J = \begin{bmatrix} 1 & 0 \\ 0 & e^{i\delta} \end{bmatrix}$$

where δ is the phase factor representing the difference between the components polarized along the b-axis and perpendicular direction.[30] The Raman intensity collected in the backscattering geometry should be expressed as

$$I \propto |e_s \cdot J \cdot R \cdot J \cdot e_i|^2 \quad (2)$$

Under parallel polarization configuration, the angular dependence of the Raman intensity of ReS_2 was then modified as

$$I_{\parallel} \propto u^2 \cos^4\theta + w^2 \sin^4\theta + 4v^2 \cos^2\theta \sin^2\theta + 2uw \cos 2\delta \cos^2\theta \sin^2\theta + 4uv \cos\delta \cos^3\theta \sin\theta + 4vw \cos\delta \cos\theta \sin^3\theta \quad (3)$$

Figure 2b show the experimental data of the angular dependence of the Raman intensities of ReS_2, which were recorded with 514.5 nm laser excitation under parallel polarization configuration. The solid curve is the fitting results using eq 1 without the consideration of the optical birefringence. Obviously, the experimental results can not be well fitted, especially the secondary minima values. However, by using eq 3, the experimental data can be nicely fitted, as shown in Figure 2c.

The phase delay due to optical birefringence is directly related to the difference in the wavelength-dependent refractive indices (Δn) along the slow and fast axes. Since the optical absorption is also related to the refractive index, we measured the anisotropic absorption of a ReS_2 sample using white light on fused silica as shown in Figure S4. Figure 2d shows the absorbance of 514.5 and 632.8 nm as a function of the angle between the polarization of the analyzer and the b-axis of ReS_2. Obviously, the absorption of this ReS_2 flake had a maximum when the polarization of the analyzer was parallel to the b-axis and had a minimum when the polarization was perpendicular. The ratio of maximum to minimum, defined as A_{max}/A_{min}, was about 1.2 for 514.5 nm, while it reached 1.5 for 632.8 nm. Apparently, the optical anisotropy is more obvious under 632.8

DOI: 10.1021/acsnano.7b05321
ACS Nano 2017, 11, 10366−10372

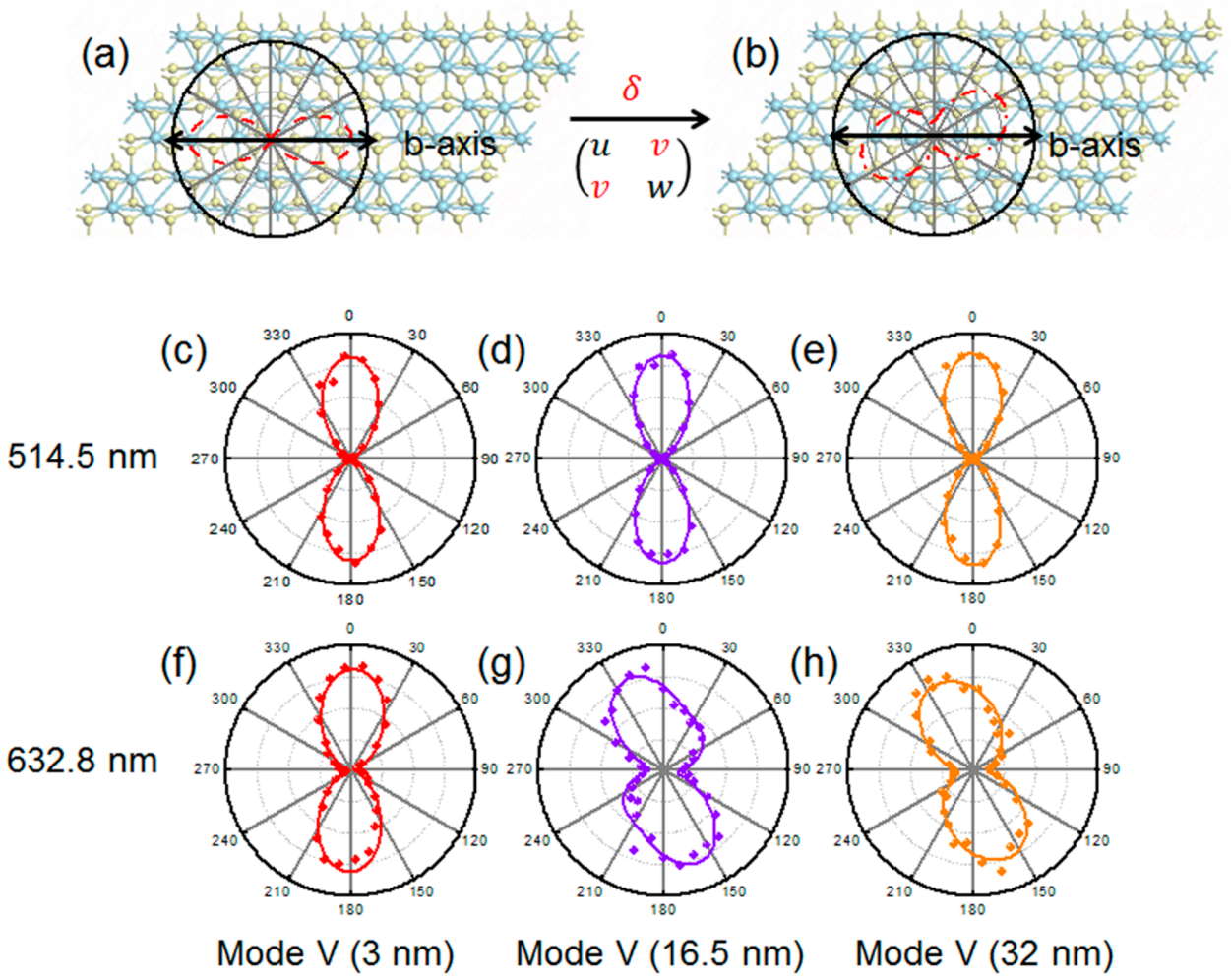

Figure 3. (a) Schematic of the method of identifying the crystalline orientation by angle-resolved polarized Raman spectra without considering the birefringence effect. (b) Schematic of the failure of identifying the crystalline orientation by angle-resolved polarized Raman spectra considering the birefringence effect. Polar plots of angle-resolved polarized Raman scattering intensities of mode V under 514.5 nm (c–e) and 632.8 nm (f–h) with a thickness of 3 nm (c, f), 16.5 nm (d, g), and 32 nm (e, h).

nm wavelength excitation. The corresponding Raman intensities of the 234.7 cm^{-1} peak (mode VI) and the curve fitting using eq 1 and eq 3 are shown in Figure 2e and f, respectively. The deviation of the curve fitting using eq 1, without considering the birefringence effect, is larger, and again, eq 3 can fit the experimental data well (Figure 2f).

For a more systematical study, angle-resolved polarized Raman scattering characterization was also performed on ReS_2 samples of different thickness using different excitation wavelengths. The polar plots of the peak intensities with different thickness are shown in Tables S1 and S2. It is notable that the polar plots showed propeller-shaped patterns. The angle difference between the maximum and the secondary maximum can deviate from 90°. This is due to the appearance of the nonzero Raman tensor element v and the phase delay factor (eqs 1–3 (SI Section 5)), in particular, the product of v cos δ, leading to the complicated angle dependence of the Raman scattering efficiency (eq 3). The phase shift (δ) is correlated to the sample thickness: $\delta = \frac{2\pi\Delta nd}{\lambda}$, where Δn is the difference of refractive index, d is the thickness of the ReS_2 flake, and λ is the laser wavelength; so with the thickness increasing, the birefringence effect would be more significant. However, the Raman tensor elements also change with thickness,[5,6] so the thickness dependence of the polarized Raman scattering feature is a net result of both the phase shift and the change of Raman tensor elements.

The quantum interpretation of the Raman selection rule is given by

$$I = \left| \sum_{i,m,m'} \frac{\langle f|\nabla|m'\rangle\langle m'|H_{\mathrm{el-ph}}|m\rangle\langle m|\nabla|i\rangle}{(E_{\mathrm{L}} - \Delta E_{mi})(E_{\mathrm{L}} - h\omega_{\nu} - \Delta E_{m'i})} \right|^2$$

where $\langle m|\nabla|i\rangle$ and $\langle f|\nabla|m'\rangle$ correspond to the electron–photon interaction in optical absorption and emission processes and $\langle m'|H_{\mathrm{el-ph}}|m\rangle$ corresponds to the electron–phonon interaction.[31] The polarization dependence of the photon–electron and electron–photon interactions is determined by the symmetry of the optical transitions.[5,10] Previous studies have shown that the electron–phonon interaction is also anisotropic, so that the net result is the product of all three items.[31] Since all the Raman modes of ReS_2 belong to A_g, the vibrational symmetry of lattice atoms should be the same for all the Raman modes, indicating the same form of electron–photon interaction. However, the different polar patterns of the modes strongly suggest the different interaction of electrons with phonons of the same symmetry.

DOI: 10.1021/acsnano.7b05321
ACS Nano 2017, 11, 10366–10372

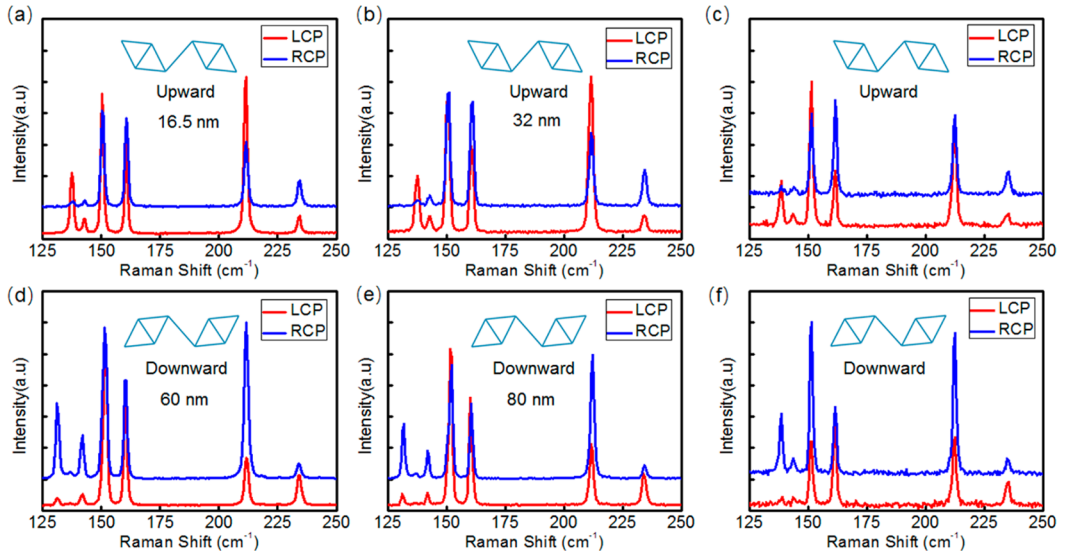

Figure 4. Raman spectra of ReS_2 flakes under left-handed circularly polarized laser (LCP) and right-handed circularly polarized laser (RCP) excitation at 514.5 nm with 16.5 nm thickness (a), 32 nm thickness (b), 60 nm thickness (d), and 80 nm thickness (e) on a SiO_2/Si substrate. Raman spectra of ReS_2 flake under LCP and RCP excitation with "upward" vertical orientation (c) and "downward" vertical orientation (f).

The identification of the crystalline axis of ReS_2 using angle-resolved polarized Raman scattering has been reported recently. The mode V (212 cm^{-1}) was used to identify the *b*-axis of mono- to few-layer ReS_2 flakes with 532 nm laser wavelength excitation.[15,21] However, care should be taken when the thickness of ReS_2 is increased and other wavelengths are used. Figure 3c–h show the polar patterns of the intensities of the 212 cm^{-1} (mode V) peak under 514.5 and 632.8 nm excitations, respectively. The *b*-axis was identified according to the cleavage edge of the sample and was set to 0°. Under 514.5 nm laser excitation, the angle of the maximal Raman intensity was almost coincident with the *b*-axis for all thicknesses, with a negligible deviation of 3°. However, the optical anisotropy is much more obvious under 632.8 nm laser excitation. With the thickness increasing, the phase shift is larger, and the Raman tensor elements have been also changed; so the maximal Raman intensity and the maximum angle are quite different. For the 3 nm thick sample, the angle of the maximal intensity was close to the *b*-axis. Owing to the more significant birefringence effect, the angles of maximal Raman intensity deviate from the *b*-axis apparently with the thickness increasing. With a thickness of 16.5 nm, there was a 20° deviation between the angle of the maximal Raman intensity and the *b*-axis and a 22° deviation with 32 nm, and the deviations were too large to be ignored. This behavior is owing to the nonzero off-diagonal Raman tensor and the phase delay. Unlike BP, the maximum angles of which are always located at the armchair or zigzag direction regardless of the sample thickness and the excitation laser wavelength, the maximum angles of ReS_2 flakes deviated significantly from the crystalline axis with different sample thicknesses and excitation laser wavelengths.

More interestingly, due to the appearance of nonzero off-diagonal Raman tensor element v and the existence of phase factor δ, layered ReS_2 showed distinctly different Raman spectra under excitation of a circularly polarized laser of left- and right-handedness. Figure 4a and b show the Raman spectra of ReS_2 of different thicknesses of 16.5 nm (a) and 32 nm (b) under 514.5 nm excitation of left-handed and right-handed circular polarization, respectively. The Raman intensities of modes I, II, and V were much larger under excitation by a left circularly polarized laser than by a right circularly polarized laser. For mode IV, the Raman intensities were larger under right circularly polarized laser excitation. This behavior can be explained by the Raman tensor and the optical anisotropy. The right-handed polarized light can be represented by a Jones vector as $\frac{\sqrt{2}}{2}[1 \quad -i]$, and the left-handed rotation light can be represented as $\frac{\sqrt{2}}{2}[1 \quad i]$. The circularly polarized light also suffers from the birefringence effect, and the Raman intensities are related to $|J \cdot R \cdot J \cdot e_i|^2$. The Raman intensity under right circularly polarized light can be expressed as

$$I^{\mathrm{R}} \propto \frac{1}{2}u^2 + v^2 + \frac{1}{2}w^2 + v(u + w)\sin\delta \tag{4}$$

and the Raman intensity under left circularly polarized light is

$$I^{\mathrm{L}} \propto \frac{1}{2}u^2 + v^2 + \frac{1}{2}w^2 - v(u + w)\sin\delta \tag{5}$$

The circular intensity differential is defined as the ratio Δ of the difference of the Raman scattered intensities in right and left circularly polarized incident light:

$$\Delta = \frac{I^{\mathrm{R}} - I^{\mathrm{L}}}{I^{\mathrm{R}} + I^{\mathrm{L}}} = \frac{2v(u + w)\sin\delta}{u^2 + 2v^2 + w^2} \tag{6}$$

According to eq 6, we see that the intensities are different if $v(u + w)\sin\delta$ is nonzero, which means that the spectral response to circular polarization excitation requires the existence of the nonzero off-diagonal element and the optical anisotropy defined by the birefringence effect, that is, the phase factor δ. The magnitude of the difference depends on the values of u, w, v, and $\sin\delta$, which differ for different Raman modes. The nonzero δ is only possible for anisotropic materials including orthorhombic, monoclinic, and triclinic crystals, and the nonzero $v(u + w)$ holds for the A_g mode of triclinic crystals and the monoclinic crystals.

It has been reported that layered ReS_2 has two vertical orientations.[15] With the "upward" orientation, the Raman tensor is $\begin{bmatrix} u & v \\ v & w \end{bmatrix}$, while with "downward" orientation, a rotation

DOI: 10.1021/acsnano.7b05321
ACS Nano 2017, 11, 10366–10372

of 180° about the *b*-axis changes the Raman tensor from $\begin{bmatrix} u & v \\ v & w \end{bmatrix}$ to $\begin{bmatrix} u & -v \\ -v & w \end{bmatrix}$. The CID of Raman scattering in ReS_2 flakes with the "downward" vertical orientation is expressed as

$$\Delta = \frac{I^R - I^L}{I^R + I^L} = \frac{-2v(u+w)\sin\delta}{u^2 + 2v^2 + w^2} \quad (7)$$

which is opposite of the ReS_2 flakes with the "upward" vertical orientation. To show the effect of the vertical orientation, the ReS_2 flakes were exfoliated on a transparent substrate, so the Raman spectra can be detected for the two different vertical orientations by flipping the sample. The optical microscopic images of the two vertical orientations are shown in Figure S12. As shown in Figure 4c, with the "upward" orientation, the Raman modes under different circularly polarized lasers showed the same tendency as the 16.5 nm thickness. When the sample was turned over, for modes I, II, and V, the Raman intensities were larger under right circularly polarized light, and for mode VI, the Raman intensities were larger under left circularly polarized light. The result of the "downward" orientation is opposite of the "upward" orientation. This phenomenon is strongly in accordance with our above analysis.

In Figure 4d and e, the circularly polarized Raman spectra of ReS_2 flakes with 60 and 80 nm sample thickness. The behaviors are coincident with the "downward" orientation, so the vertical orientation of these flakes can be determined. The value of CID in Raman scattering also changed with sample thickness (CID values of all the Raman modes are shown in Table S3 in the SI). Taking mode I as an example, the absolute values of CID were 0.82, 0.82, 0.76, and 0.65 with 16.5, 32, 60, and 80 nm sample thickness, respectively. This behavior is caused by the different phase shifts and the change of the Raman tensor elements. However, the CID is not monotonic with sample thickness increasing, because both the Raman tensor elements and the phase shifts are functions of thickness. For comparison, we also measured the circularly polarized Raman spectra of a black phosphorus flake as shown in Figure S15. As expected, due to the lack of nonzero off-diagonal Raman tensor elements, the BP flakes showed the same Raman spectra excited by the different circularly polarized light.

The Raman spectral difference, $I_R - I_L$, was shown in Figure S13. These spectra are analogous to what is known on Raman optical activity,[32,33] which measures the vibrational optical activity of chiral molecules. Nevertheless, the Raman CID in our observation is on the order of 10^{-1}, and such a high value has never been reported in the ROA of chiral molecules nor in chiral-selected surface-enhanced Raman scattering[32,33] and may indicate potential application of chiral recognition of molecules if charge interactions between the molecules and ReS_2 could occur and modulate the Raman polarizability.

CONCLUSIONS

We measured the angle-resolved polarized Raman spectra of triclinic ReS_2 flakes with different thickness under 514.5 and 632.8 nm laser wavelength excitation. The polarization dependence of ReS_2 flakes deviated from the conventional Raman selection rule. This was attributed to the existence of nonzero off-diagonal Raman tensor elements due to the triclinic symmetry and the phase factor δ due to the optical anisotropy. Furthermore, circularly polarized Raman scattering was also performed on ReS_2, and a significant CID of Raman scattering was observed. As a comparison, no Raman CID was observed on orthorhombic BP samples. The large CID provides a method to identify the vertical orientation of triclinic 2D materials. These findings may indicate potential applications in chiral recognition of molecules using 2D materials.

METHODS

Sample Preparation and Characterization. The ReS_2 samples were prepared by mechanical exfoliation from bulk ReS_2 crystals (2D Semiconductiong) on 300 nm SiO_2/Si and 1 mm fused silica substrates. An optical microscope (BX51) was used to find ReS_2 flakes on the substrate. The thickness of the ReS_2 was determined by an atomic force microscope (AFM, ICON).

Polarized Raman Measurements. Polarized Raman spectra were measured using a JY Horiba HR800 with 514.5 and 632.8 nm lasers. A 100× objective lens (0.9 NA) was used to focus the laser and collect the Raman scattered light, and a 1800 lines/mm grating was chosen for spectra acquisition. The laser power was below 100 μW to avoid damage to the ReS_2 samples. Polarizers I and II were used to select the parallel or cross-polarization configuration (Figure 1a). A quarter-wave plate was placed in the incident light path to obtain a circularly polarized laser, and no analyzer polarizer was used in the collection light path (Figure S10).

Polarized Absorption Measurements. The absorption of the ReS_2 flakes was measured in transmission mode using a Witec RSA300+ optical microscope. The ReS_2 flakes were illuminated by a KL 1500 halogen lamp (Zeiss). A 100× objective lens was used to focus the incident light, and a 60× objective lens was used to collect the signal. A polarizer before the spectrometer was used to select the collection polarization. Rotating the polarization angle of the polarizer, we obtained the angle-resolved absorption. The absorbance (A) was calculated as $A = \ln(I_0/I)$. I is the light intensity transmitted through the ReS_2 flake, and I_0 is the light intensity transmitted through the fused silica substrate.

ASSOCIATED CONTENT

Supporting Information

The Supporting Information is available free of charge on the ACS Publications website at DOI: 10.1021/acsnano.7b05321.

Crystal structure of ReS_2; detailed OM/AFM characterization of ReS_2 flakes; the ARPRS characterization of ReS_2 on different substrates; detailed discussion on the modulation of the Raman selection rules; more spectra and polar plots of experimental polarized Raman scattering; the optical layout of the circular polarized Raman spectra; more details about the circular intensity differential including the vertical orientation of ReS_2, statistic diagram, and the results of BP flakes (PDF)

AUTHOR INFORMATION

Corresponding Authors

*E-mail (L. Tong): tonglm@pku.edu.cn.
*E-mail (J. Zhang): jinzhang@pku.edu.cn.

ORCID

Lianming Tong: 0000-0001-7771-4077
Jin Zhang: 0000-0003-3731-8859

Notes

The authors declare no competing financial interest.

ACKNOWLEDGMENTS

This work is financially supported by the National Natural Science Foundation of China (NSFC) (Grant Nos. 21233001, 21790052, 51720105003, 11374355, and 21573004), the Ministry of Science and Technology (MOST) (Grant Nos. 2016YFA0200101, 2016YFA0200104, and 2015CB932400),

DOI: 10.1021/acsnano.7b05321
ACS Nano 2017, 11, 10366−10372

and the Beijing Municipal Science and Technology Planning Project (No. Z161100002116026).

REFERENCES

(1) Ferrari, A. C.; Basko, D. M. Raman Spectroscopy as a Versatile Tool for Studying the Properties of Graphene. *Nat. Nanotechnol.* **2013**, *8*, 235−246.
(2) Lu, X.; Luo, X.; Zhang, J.; Quek, S. Y.; Xiong, Q. Lattice Vibrations and Raman Scattering in Two-Dimensional Layered Materials Beyond Graphene. *Nano Res.* **2016**, *9*, 3559−3597.
(3) Zhang, X.; Qiao, X. F.; Shi, W.; Wu, J. B.; Jiang, D. S.; Tan, P. H. Phonon and Raman Scattering of Two-Dimensional Transition Metal Dichalcogenides from Monolayer, Multilayer to Bulk Material. *Chem. Soc. Rev.* **2015**, *44*, 2757−2785.
(4) Zhang, X.; Tan, Q. H.; Wu, J. B.; Shi, W.; Tan, P. H. Review on the Raman Spectroscopy of Different Types of Layered Materials. *Nanoscale* **2016**, *8*, 6435−6450.
(5) Ling, X.; Huang, S.; Hasdeo, E. H.; Liang, L.; Parkin, W. M.; Tatsumi, Y.; Nugraha, A. R.; Puretzky, A. A.; Das, P. M.; Sumpter, B. G.; Geohegan, D. B.; Kong, J.; Saito, R.; Drndic, M.; Meunier, V.; Dresselhaus, M. S. Anisotropic Electron-Photon and Electron-Phonon Interactions in Black Phosphorus. *Nano Lett.* **2016**, *16*, 2260−2267.
(6) Ribeiro, H. B.; Pimenta, M. A.; De Matos, C. J.; Moreira, R. L.; Rodin, A. S.; Zapata, J. D.; De Souza, E. A.; Castro Neto, A. H. Unusual Angular Dependence of the Raman Response in Black Phosphorus. *ACS Nano* **2015**, *9*, 4270−4276.
(7) Wu, J.; Mao, N.; Xie, L.; Xu, H.; Zhang, J. Identifying the Crystalline Orientation of Black Phosphorus Using Angle-Resolved Polarized Raman Spectroscopy. *Angew. Chem., Int. Ed.* **2015**, *54*, 2366−2369.
(8) Song, Q.; Pan, X.; Wang, H.; Zhang, K.; Tan, Q.; Li, P.; Wan, Y.; Wang, Y.; Xu, X.; Lin, M.; Wan, X.; Song, F.; Dai, L. The In-Plane Anisotropy of WTe_2 Investigated by Angle-Dependent and Polarized Raman Spectroscopy. *Sci. Rep.* **2016**, *6*, 29254.
(9) Tian, Z.; Guo, C.; Zhao, M.; Li, R.; Xue, J. Two-Dimensional SnS: A Phosphorene Analogue with Strong In-Plane Electronic Anisotropy. *ACS Nano* **2017**, *11*, 2219−2226.
(10) Huang, S.; Tatsumi, Y.; Ling, X.; Guo, H.; Wang, Z.; Watson, G.; Puretzky, A. A.; Geohegan, D. B.; Kong, J.; Li, J.; Yang, T.; Saito, R.; Dresselhaus, M. S. In-Plane Optical Anisotropy of Layered Gallium Telluride. *ACS Nano* **2016**, *10*, 8964−8972.
(11) Chen, S. Y.; Zheng, C.; Fuhrer, M. S.; Yan, J. Helicity-Resolved Raman Scattering of MoS_2, $MoSe_2$, WS_2, and WSe_2 Atomic Layers. *Nano Lett.* **2015**, *15*, 2526−2532.
(12) Loudon, R. The Raman Effect in Crystals. *Adv. Phys.* **2001**, *50*, 813−864.
(13) Lorchat, E.; Froehlicher, G.; Berciaud, S. Splitting of Interlayer Shear Modes and Photon Energy Dependent Anisotropic Raman Response in N-Layer $ReSe_2$ and ReS_2. *ACS Nano* **2016**, *10*, 2752−2760.
(14) Ma, X.; Guo, P.; Yi, C.; Yu, Q.; Zhang, A.; Ji, J.; Tian, Y.; Jin, F.; Wang, Y.; Liu, K.; Xia, T.; Shi, Y.; Zhang, Q. Raman Scattering in the Transition-Metal Dichalcogenides of 1T′−$MoTe_2$,T_d−$MoTe_2$, and T_d−WTe_2. *Phys. Rev. B: Condens. Matter Mater. Phys.* **2016**, *94*, 214105.
(15) Hart, L.; Dale, S.; Hoye, S.; Webb, J. L.; Wolverson, D. Rhenium Dichalcogenides: Layered Semiconductors with Two Vertical Orientations. *Nano Lett.* **2016**, *16*, 1381−6.
(16) Mao, N.; Wu, J.; Han, B.; Lin, J.; Tong, L.; Zhang, J. Birefringence-Directed Raman Selection Rules in 2D Black Phosphorus Crystals. *Small* **2016**, *12*, 2627−33.
(17) Corbet, C. M.; McClellan, C.; Rai, A.; Sonde, S. S.; Tutuc, E.; Banerjee, S. K. Field Effect Transistors with Current Saturation and Voltage Gain in Ultrathin ReS_2. *ACS Nano* **2014**, *9*, 363−370.
(18) Ovchinnikov, D.; Gargiulo, F.; Allain, A.; Pasquier, D. J.; Dumcenco, D.; Ho, C. H.; Yazyev, O. V.; Kis, A. Disorder Engineering and Conductivity Dome in ReS_2 with Electrolyte Gating. *Nat. Commun.* **2016**, *7*, 12391.
(19) Liu, F.; Zheng, S.; He, X.; Chaturvedi, A.; He, J.; Chow, W. L.; Mion, T. R.; Wang, X.; Zhou, J.; Fu, Q.; Fan, H. J.; Tay, B. K.; Song, L.; He, R.-H.; Kloc, C.; Ajayan, P. M.; Liu, Z. Highly Sensitive Detection of Polarized Light Using Anisotropic 2D ReS_2. *Adv. Funct. Mater.* **2016**, *26*, 1169−1177.
(20) Aslan, O. B.; Chenet, D. A.; van der Zande, A. M.; Hone, J. C.; Heinz, T. F. Linearly Polarized Excitons in Single- and Few-Layer ReS_2 Crystals. *ACS Photonics* **2016**, *3*, 96−101.
(21) Chenet, D. A.; Aslan, O. B.; Huang, P. Y.; Fan, C.; van der Zande, A. M.; Heinz, T. F.; Hone, J. C. In-Plane Anisotropy in Mono- and Few-Layer ReS_2 Probed by Raman Spectroscopy and Scanning Transmission Electron Microscopy. *Nano Lett.* **2015**, *15*, 5667−5672.
(22) He, R.; Yan, J. A.; Yin, Z.; Ye, Z.; Ye, G.; Cheng, J.; Li, J.; Lui, C. H. Coupling and Stacking Order of ReS_2 Atomic Layers Revealed by Ultralow-Frequency Raman Spectroscopy. *Nano Lett.* **2016**, *16*, 1404−1409.
(23) Qiao, X. F.; Wu, J. B.; Zhou, L.; Qiao, J.; Shi, W.; Chen, T.; Zhang, X.; Zhang, J.; Ji, W.; Tan, P. H. Polytypism and Unexpected Strong Interlayer Coupling in Two-Dimensional layered ReS_2. *Nanoscale* **2016**, *8*, 8324−8332.
(24) Tongay, S.; Sahin, H.; Ko, C.; Luce, A.; Fan, W.; Liu, K.; Zhou, J.; Huang, Y. S.; Ho, C. H.; Yan, J.; Ogletree, D. F.; Aloni, S.; Ji, J.; Li, S.; Li, J.; Peeters, F. M.; Wu, J. Monolayer Behaviour in Bulk ReS_2 Due to Electronic and Vibrational Decoupling. *Nat. Commun.* **2014**, *5*, 3252.
(25) Feng, Y.; Zhou, W.; Wang, Y.; Zhou, J.; Liu, E.; Fu, Y.; Ni, Z.; Wu, X.; Yuan, H.; Miao, F.; Wang, B.; Wan, X.; Xing, D. Raman Vibrational Spectra of Bulk to Monolayer ReS_2 with Lower Symmetry. *Phys. Rev. B: Condens. Matter Mater. Phys.* **2015**, *92*, 054110.
(26) Kelty, S. P.; Ruppert, A. F.; Chianelli, R. R.; Ren, J.; Whangbo, M.-H. Scanning Probe Microscopy Study of Layered Dichalcogenide ReS_2. *J. Am. Chem. Soc.* **1994**, *116*, 7857−7863.
(27) Cui, F.; Wang, C.; Li, X.; Wang, G.; Liu, K.; Yang, Z.; Feng, Q.; Liang, X.; Zhang, Z.; Liu, S.; Lei, Z.; Liu, Z.; Xu, H.; Zhang, J. Tellurium-Assisted Epitaxial Growth of Large-Area, Highly Crystalline ReS_2 Atomic Layers on Mica Substrate. *Adv. Mater.* **2016**, *28*, 5019−5024.
(28) Hafeez, M.; Gan, L.; Li, H.; Ma, Y.; Zhai, T. Large-Area Bilayer ReS_2 Film/Multilayer ReS_2 Flakes Synthesized by Chemical Vapor Deposition for High Performance Photodetectors. *Adv. Funct. Mater.* **2016**, *26*, 4551−4560.
(29) Wu, K.; Chen, B.; Yang, S.; Wang, G.; Kong, W.; Cai, H.; Aoki, T.; Soignard, E.; Marie, X.; Yano, A.; Suslu, A.; Urbaszek, B.; Tongay, S. Domain Architectures and Grain Boundaries in Chemical Vapor Deposited Highly Anisotropic ReS_2 Monolayer Films. *Nano Lett.* **2016**, *16*, 5888−5894.
(30) Jones, R. C. A New Calculus for the Treatment of Optical Systems I. Description and Discussion of the Calculus. *J. Opt. Soc. Am.* **1941**, *31*, 488−493.
(31) Saito, R.; Tatsumi, Y.; Huang, S.; Ling, X.; Dresselhaus, M. S. Raman Spectroscopy of Transition Metal Dichalcogenides. *J. Phys.: Condens. Matter* **2016**, *28*, 353002.
(32) Barron, L. D.; Buckingham, A. D. Rayleigh and Raman Scattering from Optically Active Molecules. *Mol. Phys.* **1971**, *20*, 1111−1119.
(33) Ostovar pour, S.; Rocks, L.; Faulds, K.; Graham, D.; Parchansky, V.; Bour, P.; Blanch, E. W. Through-Space Transfer of Chiral Information Mediated by a Plasmonic Nanomaterial. *Nat. Chem.* **2015**, *7*, 591−596.

DOI: 10.1021/acsnano.7b05321
ACS Nano 2017, 11, 10366−10372